

# Neutrino Nucleosynthesis of radioactive nuclei in supernovae

A. Sieverding,<sup>1</sup> L. Huther,<sup>1</sup> K. Langanke,<sup>2,1</sup> G. Martínez-Pinedo,<sup>1,2</sup> and A. Heger<sup>3,4,5,6</sup>

<sup>1</sup>*Institut für Kernphysik (Theoriezentrum), Technische Universität Darmstadt,  
Schlossgartenstraße 2, 64289 Darmstadt, Germany*

<sup>2</sup>*Gesellschaft für Schwerionenforschung Darmstadt, Planckstr. 1, D-64259 Darmstadt, Germany*

<sup>3</sup>*Monash Centre for Astrophysics, School of Physics and Astronomy, Monash University, Victoria 3800, Australia*

<sup>4</sup>*University of Minnesota, School of Physics and Astronomy, Minneapolis, MN 55455, USA*

<sup>5</sup>*Shanghai Jiao-Tong University, CNA, Department of Physics and Astronomy, Shanghai 200240, P.R. China*

<sup>6</sup>*The Joint Institute for Nuclear Astrophysics*

We study the neutrino-induced production of nuclides in explosive supernova nucleosynthesis for progenitor stars with solar metallicity and initial main sequence masses between  $15 M_{\odot}$  and  $40 M_{\odot}$ . We improve previous investigations i) by using a global set of partial differential cross sections for neutrino-induced charged- and neutral-current reactions on nuclei with charge numbers  $Z < 76$  and ii) by considering modern supernova neutrino spectra which have substantially lower average energies compared to those previously adopted in neutrino nucleosynthesis studies. We confirm the production of  ${}^7\text{Li}$ ,  ${}^{11}\text{B}$ ,  ${}^{138}\text{La}$ , and  ${}^{180}\text{Ta}$  by neutrino nucleosynthesis, albeit at slightly smaller abundances due to the changed neutrino spectra. We find that for stars with a mass smaller than  $20 M_{\odot}$ ,  ${}^{19}\text{F}$  is produced mainly by explosive nucleosynthesis while for higher mass stars it is produced by the  $\nu$  process. We also find that neutrino-induced reactions, either directly or indirectly by providing an enhanced abundance of light particles, noticeably contribute to the production of the radioactive nuclides  ${}^{22}\text{Na}$  and  ${}^{26}\text{Al}$ . Both nuclei are prime candidates for gamma-ray astronomy. Other prime targets,  ${}^{44}\text{Ti}$  and  ${}^{60}\text{Fe}$ , however, are insignificantly produced by neutrino-induced reactions. We also find a large increase in the production of the long-lived nuclei  ${}^{92}\text{Nb}$  and  ${}^{98}\text{Tc}$  due to charged-current neutrino capture.

PACS numbers: 26.30.Jk, 25.30.Pt, 26.30.Ef

Astrophysical objects like stars, novae, or supernovae are the origin of most of the elements in the Universe [1, 2]. Whereas the likely nucleosynthesis processes associated with these objects have been identified and a general understanding has been developed, many details of their operation are still unresolved [3–5]. This is due to limited computational capabilities to simulate astrophysical objects and to the fact that the properties of the nuclides involved in the nucleosynthesis processes are not known experimentally and have to be modeled [6].

Detections of gamma-rays from radioactive nuclei by space bound observatories like INTEGRAL [7] are an invaluable tool to determine their production sites and thereby advance our understanding of astrophysical nucleosynthesis. Such detection allows for a snapshot view of the ongoing nucleosynthesis in our galaxy and, provided a suited nuclear half-life, to relate the origin of the nuclide to a specific astrophysical source [8]. In cases where the observation can be assigned to a particular supernova remnant, one can learn about asymmetries in the explosion [9]. The prime nuclide for gamma-ray astronomy in recent years has been  ${}^{26}\text{Al}$  [10]. Its production has been associated with several astrophysical sources (see ref. [11] and references therein), however, in recent years evidence has been brought forward [10, 12, 13] that massive stars can account for most of the  ${}^{26}\text{Al}$  in the galaxy. Other gamma-ray astronomy candidates like  ${}^{22}\text{Na}$ ,  ${}^{44}\text{Ti}$ , and  ${}^{60}\text{Fe}$  are also related to core-collapse supernovae [12, 14–17].

It has long been recognized that, in the  $\nu$  process during a supernova explosion, neutrino-nucleus reactions are essential for the synthesis of selected nuclides like  ${}^7\text{Li}$ ,  ${}^{11}\text{B}$ ,  ${}^{15}\text{N}$ ,  ${}^{19}\text{F}$ ,  ${}^{138}\text{La}$ , or  ${}^{180}\text{Ta}$  [11, 18] or can contribute to the production of long lived radioactive nuclides [11, 12, 16, 17]. In the  $\nu$  process neutrinos of all flavors, which are emitted by the cooling proto-neutron star (PNS), interact with nuclei as they pass through the surrounding stellar matter. At the same time, these outer layers are heated up and compressed by the explosion shockwave propagating outward from the PNS and causing the ejection of the material. Neutral-current reactions excite the nucleus to states above particle thresholds so that the subsequent decay is accompanied by emission of light particles (proton, neutron or  $\alpha$  particle). Due to the relatively low energies of the neutrinos, charged-current reactions can only be induced by electron-type neutrinos. This process can be accompanied by light-particle emission if the  $(\nu_e, e^-)$  or  $(\bar{\nu}_e, e^+)$  reactions excite the daughter nucleus to levels above particle thresholds. Hence selected nuclei, e.g.  ${}^{11}\text{B}$ ,  ${}^{19}\text{F}$ ,  ${}^{138}\text{La}$ , and  ${}^{180}\text{Ta}$ , are produced directly as daughter products of neutrino-induced reactions. The abundance of other nuclides, e.g.  ${}^7\text{Li}$ , is enhanced indirectly by neutrino spallation reactions as these increase the amount of light particles required to synthesize these nuclides within a network of charged-particle reactions.

The focus of this letter is to explore the impact of the  $\nu$  process on the production of long-lived radioactive

nuclei of interest to gamma-ray astronomy. Previous investigations of nucleosynthesis by neutrino-induced reactions have been based on stellar simulations using various hydrodynamical models [11, 15, 18] using neutrino-nucleus cross section data which were restricted to a set of key nuclei (like those which are quite abundant in outer burning shells) and to a limited number of decay channels. Furthermore, the simulations adopted supernova neutrino energy spectra, described by Fermi-Dirac distributions with chemical potential  $\mu = 0$  and temperature  $T_\nu$ , which were appropriate at the time the studies were performed; i.e.  $T_{\nu_e, \bar{\nu}_e} = 4\text{-}5$  MeV for electron (anti-)neutrinos, corresponding to average energies,  $\langle E_\nu \rangle = 3.15 T_\nu$ , between 12 MeV and 16 MeV [11, 18] and  $T_{\nu_\mu, \tau} = 5\text{-}10$  MeV [11, 12, 18] for muon and tau neutrinos as well as for the corresponding anti-neutrinos, corresponding to average energies between 16 MeV and 32 MeV. We improve these simulations in two relevant aspects. Firstly, we have derived a complete set of partial differential cross sections for neutrino-induced charged- and neutral-current reactions on the global chart of nuclei for charge numbers  $Z < 76$  considering various single- and multi-particle decay channels. Secondly, the more realistic treatment of neutrino transport in recent supernova simulations [19–21] yield spectra for all neutrino families which are noticeably shifted to lower energies. This reduces the neutrino-nucleus cross sections; in particular particle spallation cross sections for neutral-current reactions which are very sensitive to the tail of the neutrino spectra. Our choice of neutrino temperatures is  $T_{\nu_e} = 2.8$  MeV,  $T_{\bar{\nu}_e} = T_{\nu_\mu, \tau} = 4.0$  MeV based on recent simulations [19–21].

We have calculated partial differential neutrino-nucleus cross sections globally for nuclei with  $Z < 76$  based on a two-step strategy [22]: i) the neutrino-induced nuclear excitation cross sections to a final state at energy  $E$  have been calculated within the Random Phase Approximation (following [23]) allowing for partial proton and neutron occupancies and considering multipole transitions up to order  $\lambda = 4$ . The single particle energies were adopted from an appropriate Woods-Saxon parametrization, adjusted to reproduce the proton and neutron thresholds and to account for the energies of the Isobaric Analog State and the leading giant resonances. ii) The decay probabilities of the excited nuclear levels have been derived within the statistical model. At low excitation energies we use a Modified Smoker code [24] which considers experimentally known states and their properties explicitly and then matches the experimental spectrum to a level density. The code is restricted to treat single-particle decays. To allow for multi-particle decay, which becomes relevant at modest excitation energies or in nuclei with large neutron excess and hence small separation energies, we have adopted the ABLA code [25] at higher excitation energies, which has been well validated to properly describe multi-particle decays

and fission. The results of the two statistical model codes have been smoothly matched at moderate energies above the single-particle thresholds. In the reaction network all neutrino-induced reactions on nuclei with charge number  $Z < 76$  are included. This gives a consistent picture of  $\nu$ -nucleosynthesis covering the whole range of nuclei from light to heavy. Crucial cross-sections for  ${}^4\text{He}$  are taken from reference [26] and for  ${}^{12}\text{C}$  the values used in reference [11] are adopted. Our cross sections for  ${}^{20}\text{Ne}$  and  ${}^{138}\text{Ba}$  and  ${}^{180}\text{Hf}$  are consistent with experimental constraints [18, 27].

The evolution of the shockwave passing through the outer layers of the star is described using the parametrization of ref. [11]. It reproduces hydrodynamical calculations [16] particularly for the peak temperature reached as the shock passes. This temperature is the key quantity for nucleosynthesis. The parametrization assumes that the region behind the shock is radiation dominated, containing the kinetic explosion energy of  $10^{51}$  erg. The neutrino luminosity is modeled following reference [11]. It assumes a total energy of  $3 \times 10^{53}$  ergs equally distributed in all neutrino flavors. For a particular neutrino flavor the luminosity is assumed to decay exponentially with a timescale of 3 s, i.e.  $L_\nu = 5/3 \times 10^{52} \exp(-t/3)$  erg s $^{-1}$  with  $t$  in seconds. The composition is followed with a reaction network including all relevant nuclei and reactions up charge number  $Z = 76$ . The abundances are evolved up to  $2.5 \times 10^4$  s after bounce. We have used pre-supernova progenitor models from ref. [17, 28] in the mass range 15–40  $M_\odot$ . It is unclear which of the explored models will explode and how the explosion energy and amount of fallback depend on progenitor mass and structure [29–32]. We find that the  $\nu$  process mainly operates in outer regions of the stellar mantle that should not be affected by fallback. Nevertheless, fallback may trigger the formation of a black hole resulting in a sudden end of neutrino emission [33] This possibility is neglected in our calculations.

The main candidates for neutrino nucleosynthesis are  ${}^7\text{Li}$ ,  ${}^{11}\text{B}$ ,  ${}^{15}\text{N}$ ,  ${}^{19}\text{F}$ ,  ${}^{138}\text{La}$ , and  ${}^{180}\text{Ta}$  [18], all of which are observed in the solar system, but are not produced in sufficient amount by supernova simulations without including neutrino interactions. Neutrino nucleosynthesis pushes the production factors of those nuclei close to the solar system values (Table I). The relative increase of  ${}^7\text{Li}$  and  ${}^{11}\text{B}$  is strongly affected by the  $\nu$  process. At the base of the He-shell the neutral current neutrino-interactions  ${}^4\text{He}(\nu, \nu'p)$  and  ${}^4\text{He}(\nu, \nu'n)$  contribute to produce  ${}^7\text{Li}$  by the reactions  ${}^3\text{He}(\alpha, \gamma){}^7\text{Be}(\beta^+){}^7\text{Li}$  and  ${}^{11}\text{B}$  via  ${}^3\text{H}(\alpha, \gamma){}^7\text{Li}(\alpha, \gamma){}^{11}\text{B}$ . The yields obtained in our calculations are consistent with reference [18], although our neutrino energies are substantially lower. We find that  ${}^{11}\text{B}$  can be produced in full solar abundance, whereas  ${}^7\text{Li}$  is still underproduced, supporting the need for other sources of  ${}^7\text{Li}$  [35].

Reference [18] states that the  $\nu$  process can probably

TABLE I. Production factors relative to solar abundances from reference [34], normalized to  $^{16}\text{O}$  production. Shown are the results obtained without neutrino, with our choice of neutrino temperatures (“Low energies”), and with the choice of ref. [18] (“High energies”).

Star	Nucleus	no $\nu$	Low energies <sup>a</sup>	High energies <sup>b</sup>
15 $M_{\odot}$	$^7\text{Li}$	0.001	0.28	2.54
	$^{11}\text{B}$	0.007	1.43	6.13
	$^{15}\text{N}$	0.67	0.68	0.79
	$^{19}\text{F}$	1.02	1.14	1.31
	$^{138}\text{La}$	0.07	0.67	1.18
	$^{180}\text{Ta}$	0.07	1.14	1.81
25 $M_{\odot}$	$^7\text{Li}$	0.0005	0.11	0.55
	$^{11}\text{B}$	0.003	0.80	2.61
	$^{15}\text{N}$	0.08	0.10	0.13
	$^{19}\text{F}$	0.06	0.24	0.43
	$^{138}\text{La}$	0.03	0.63	1.14
	$^{180}\text{Ta}$	0.14	1.80	2.81

<sup>a</sup>  $T_{\nu_e} = 2.8$  MeV,  $T_{\bar{\nu}_e} = T_{\nu_{\mu,\tau}} = 4.0$  MeV

<sup>b</sup>  $T_{\nu_e} = T_{\bar{\nu}_e} = 4.0$  MeV,  $T_{\nu_{\mu,\tau}} = 6.0$  MeV

not account for the entire solar abundance of  $^{19}\text{F}$ . We find that the mechanism for its production is rather different for the low mass and high mass progenitors considered here. For the 15  $M_{\odot}$  model, the ratio  $^{19}\text{F}/^{16}\text{O}$  is consistent with solar proportions even without neutrinos. The pre-supernova  $^{19}\text{F}/^{16}\text{O}$  ratio of 0.07 is increased to a final value of 1.14 during shock passage mainly by the reaction sequence  $^{18}\text{O}(p, \alpha)^{15}\text{N}(\alpha, \gamma)^{19}\text{F}$  operating on  $^{18}\text{O}$  at the lower edge of the He-shell where post shock temperatures reach values up to 0.7 GK at densities of up to  $1500 \text{ g cm}^{-3}$ . The temperature and density reached in this region depends on the radial position of the shell interface and hence is very sensitive to the progenitor structure. Reference [17] discusses the major changes of stellar structure that appear for stars between 15 and 25  $M_{\odot}$ . In particular, we find that for stars with a mass smaller than 20  $M_{\odot}$   $^{19}\text{F}$  is produced mainly by explosive nucleosynthesis, whereas for higher mass stars it is produced by the  $\nu$  process (Table II). Given the uncertainties involved in stellar modeling, arising especially from the treatment of convection and uncertainties in nuclear reaction rates at astrophysical energies, the production of  $^{19}\text{F}$  up to solar abundance cannot be excluded by our calculations. To address the sensitivity to the progenitor structure, we have explored the production of  $^{19}\text{F}$  based on models from ref. [15, 36] and found similar enhancement in the production factors of  $^{19}\text{F}$  for low mass stars with substantial quantitative differences with respect to the yields presented here. Our results for  $^{138}\text{La}$  and  $^{180}\text{Ta}$  are consistent with those of refs. [18, 27].

Table II lists the nucleosynthesis yields for those nuclei that are affected by the  $\nu$  process including long lived

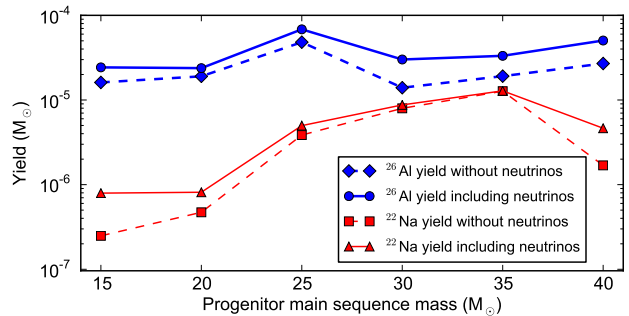


FIG. 1. Yields of  $^{26}\text{Al}$  (thick blue lines with circles) and  $^{22}\text{Na}$  (thin red lines with triangles) for the set of progenitor stars considered. Given is the yield without neutrinos (dashed lines) and including neutrinos with  $T_{\nu_e} = 2.8$  MeV and  $T_{\bar{\nu}_e} = T_{\nu_{\mu,\tau}} = 4$  MeV.

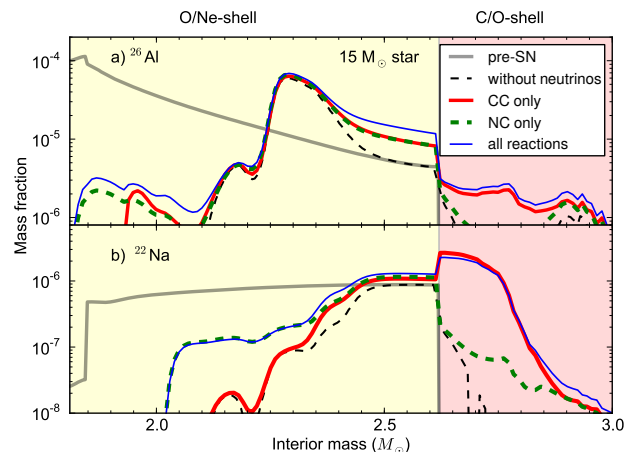


FIG. 2. Mass fraction of  $^{26}\text{Al}$  (upper panel) and  $^{22}\text{Na}$  (lower panel) for the same 15  $M_{\odot}$  main sequence mass progenitor star of solar metallicity. Shown are the results for calculations with and without including neutrino interactions, with charged-current reactions only, and neutral-current reactions only. The pre-supernova mass fractions are also shown.

radioactive nuclei. The yields of short-lived radioactive nuclei, e.g.  $^{32}\text{P}$ ,  $^{72}\text{As}$ ,  $^{84}\text{Rb}$ ,  $^{88}\text{Y}$  are increased by factors between 10 and 100. Their lifetimes are of the order of a 100 days or shorter, putting their decay signal in competition with  $^{56}\text{Ni}$  and its daughter  $^{56}\text{Co}$  which by far dominates the early lightcurve and therefore outshines the signature of the  $\nu$  process. The typical yields for  $^{72}\text{As}$ ,  $^{84}\text{Rb}$ , and  $^{88}\text{Y}$  are  $10^{-8} M_{\odot}$ , which may allow for the observation of the gamma-ray decay lines. We also find a significant enhancement of the production of the long-lived isotope  $^{36}\text{Cl}$  which, however, decays mainly to the ground-state of  $^{36}\text{Ar}$  without characteristic  $\gamma$ -rays. The yield of  $^{26}\text{Al}$  is known to be enhanced by neutrino nucleosynthesis [11, 12]. We find that the yield of  $^{26}\text{Al}$  is increased by factors between 1.25 and 2.51 in

TABLE II. Yields of different radioactive nuclei and the effects of the  $\nu$ -process for different progenitor stars. Shown are the results for the calculations without including neutrino interactions (“no  $\nu$ ”) and the results including neutrinos.

nucleus	15 $M_{\odot}$		20 $M_{\odot}$		25 $M_{\odot}$		30 $M_{\odot}$	
	no $\nu$	$\nu$						
${}^6\text{Li}$	$5.46 \times 10^{-11}$	$5.65 \times 10^{-11}$	$4.24 \times 10^{-17}$	$5.01 \times 10^{-12}$	$8.78 \times 10^{-11}$	$9.87 \times 10^{-11}$	$1.04 \times 10^{-10}$	$1.24 \times 10^{-10}$
${}^7\text{Li}$	$1.44 \times 10^{-09}$	$1.04 \times 10^{-07}$	$5.29 \times 10^{-14}$	$1.84 \times 10^{-07}$	$2.35 \times 10^{-09}$	$7.25 \times 10^{-08}$	$2.74 \times 10^{-09}$	$8.89 \times 10^{-08}$
${}^9\text{Be}$	$5.22 \times 10^{-11}$	$7.09 \times 10^{-11}$	$2.73 \times 10^{-19}$	$8.81 \times 10^{-12}$	$8.01 \times 10^{-11}$	$1.15 \times 10^{-10}$	$9.16 \times 10^{-11}$	$1.17 \times 10^{-10}$
${}^{10}\text{B}$	$1.15 \times 10^{-09}$	$2.06 \times 10^{-09}$	$1.60 \times 10^{-10}$	$5.34 \times 10^{-10}$	$2.09 \times 10^{-09}$	$3.84 \times 10^{-09}$	$2.29 \times 10^{-09}$	$3.42 \times 10^{-09}$
${}^{11}\text{B}$	$3.70 \times 10^{-09}$	$1.10 \times 10^{-07}$	$6.74 \times 10^{-11}$	$2.23 \times 10^{-07}$	$6.33 \times 10^{-09}$	$1.97 \times 10^{-07}$	$7.20 \times 10^{-09}$	$1.26 \times 10^{-07}$
${}^{19}\text{F}$	$6.10 \times 10^{-05}$	$6.43 \times 10^{-05}$	$6.94 \times 10^{-06}$	$8.24 \times 10^{-06}$	$1.40 \times 10^{-05}$	$5.53 \times 10^{-05}$	$9.19 \times 10^{-05}$	$1.32 \times 10^{-04}$
${}^{22}\text{Na}$	$2.48 \times 10^{-07}$	$7.50 \times 10^{-07}$	$4.71 \times 10^{-07}$	$8.13 \times 10^{-07}$	$3.85 \times 10^{-06}$	$4.94 \times 10^{-06}$	$7.97 \times 10^{-06}$	$8.71 \times 10^{-06}$
${}^{26}\text{Al}$	$1.61 \times 10^{-05}$	$2.43 \times 10^{-05}$	$1.89 \times 10^{-05}$	$2.36 \times 10^{-05}$	$5.10 \times 10^{-05}$	$7.11 \times 10^{-05}$	$2.02 \times 10^{-05}$	$3.63 \times 10^{-05}$
${}^{36}\text{Cl}$	$5.64 \times 10^{-07}$	$2.22 \times 10^{-05}$	$1.11 \times 10^{-04}$	$1.34 \times 10^{-04}$	$4.78 \times 10^{-06}$	$5.23 \times 10^{-05}$	$1.30 \times 10^{-06}$	$3.55 \times 10^{-05}$
${}^{44}\text{Ti}$	$1.09 \times 10^{-04}$	$1.23 \times 10^{-04}$	$5.38 \times 10^{-05}$	$6.15 \times 10^{-05}$	$1.13 \times 10^{-04}$	$1.09 \times 10^{-04}$	$5.67 \times 10^{-05}$	$7.84 \times 10^{-05}$
${}^{60}\text{Fe}$	$1.35 \times 10^{-04}$	$1.40 \times 10^{-04}$	$3.55 \times 10^{-05}$	$3.55 \times 10^{-05}$	$1.60 \times 10^{-04}$	$1.50 \times 10^{-04}$	$7.23 \times 10^{-05}$	$7.49 \times 10^{-05}$
${}^{92}\text{Nb}$	$2.15 \times 10^{-12}$	$4.09 \times 10^{-11}$	$6.59 \times 10^{-10}$	$7.64 \times 10^{-10}$	$9.54 \times 10^{-11}$	$6.05 \times 10^{-10}$	$4.58 \times 10^{-12}$	$4.27 \times 10^{-10}$
${}^{98}\text{Tc}$	$1.12 \times 10^{-11}$	$1.37 \times 10^{-11}$	$1.11 \times 10^{-11}$	$3.31 \times 10^{-11}$	$1.11 \times 10^{-11}$	$5.89 \times 10^{-11}$	$1.74 \times 10^{-12}$	$4.07 \times 10^{-11}$
${}^{138}\text{La}$	$1.34 \times 10^{-11}$	$1.32 \times 10^{-10}$	$2.11 \times 10^{-10}$	$3.07 \times 10^{-10}$	$2.79 \times 10^{-11}$	$5.17 \times 10^{-10}$	$2.97 \times 10^{-11}$	$4.15 \times 10^{-10}$
${}^{180}\text{Ta}$	$7.89 \times 10^{-14}$	$1.85 \times 10^{-12}$	$1.49 \times 10^{-13}$	$2.32 \times 10^{-12}$	$8.09 \times 10^{-13}$	$1.23 \times 10^{-11}$	$3.05 \times 10^{-13}$	$1.31 \times 10^{-11}$

the range of progenitor models studied (see Table II and Figure 1). The production of  ${}^{26}\text{Al}$  during the explosion occurs mostly in a narrow region of the O/Ne shell, in which  ${}^{26}\text{Mg}$  and  ${}^{25}\text{Mg}$  are abundant and the post-shock temperature is below 2 GK. Deeper layers are subject to higher peak temperatures such that the  ${}^{26}\text{Al}$  produced before the explosion is destroyed by  ${}^{26}\text{Al}(p, \gamma)$ . Neutrinos contribute to the production of  ${}^{26}\text{Al}$  during the explosive phase by two different mechanisms. Neutrino-induced spallation reactions on the most abundant nuclei in the O/Ne shell,  ${}^{20}\text{Ne}$ ,  ${}^{24}\text{Mg}$ , and  ${}^{16}\text{O}$  increase the number of free protons, enhancing the reaction  ${}^{25}\text{Mg}(p, \gamma)$ , which is also the main production channel without neutrinos. Additionally, the charged-current reaction  ${}^{26}\text{Mg}(\nu_e, e^-)$  gives significant contributions. Figure 2 illustrates the different production channels for the 15  $M_{\odot}$  progenitor model. Compared with previous studies, we find a reduction of the neutral-current channel due to the reduced neutrino energies. Hence, both charged- and neutral-current reactions contribute to a similar extent to the production of  ${}^{26}\text{Al}$  in the O/Ne layer. The enhancement of the  ${}^{25}\text{Mg}(p, \gamma)$  is confined to a narrow region of optimal temperature, whereas the  ${}^{26}\text{Mg}(\nu_e, e^-)$  contributes more evenly throughout the entire layer, decreasing with the neutrino flux at larger radii.

Our 20  $M_{\odot}$  progenitor suffers an early merging of the convective O-, Ne-, and C-shells which significantly changes the chemical composition of this model [17] and depletes the progenitor abundances of  ${}^{26}\text{Mg}$  and  ${}^{25}\text{Mg}$ . Consequently, the yield of  ${}^{26}\text{Al}$  is reduced. The 25  $M_{\odot}$  progenitor exhibits the largest compactness, i.e., the mass over radius ratio for a particular enclosed mass,

and therefore provides the most favorable conditions for the production of  ${}^{26}\text{Al}$ . Due to higher temperatures and more convective mixing during their evolution, less  ${}^{26}\text{Al}$  remains from the hydrostatic burning stages. However, the efficiency of the  $\nu$  process is enhanced, because of large densities in the O/Ne shell.

The radioisotope  ${}^{22}\text{Na}$  (Figure 2) is also affected by neutral and charged current reactions.  ${}^{21}\text{Ne}(p, \gamma)$  which occurs in the O/Ne shell is enhanced by neutral-current neutrino-induced spallation reactions and the charged-current  ${}^{22}\text{Ne}(\nu_e, e^-)$  provides a direct production channel in the C/O layer, where  ${}^{22}\text{Ne}$  has been produced during the He-burning phases. Compared with previous studies, the charged-current contribution turns out to be more important for all the progenitors studied here due to the lower neutrino energies. The total yield is increased due to neutrinos by up to a factor of 3 (see Figure 1 and Table II). This effect is very dependent on the initial conditions provided by the progenitor and almost disappears for the 35  $M_{\odot}$  model. Since the different production channels occur in spatially separated layers of the star, the relative weight strongly depends on the position of the shell interfaces and is therefore also sensitive to the details of the stellar evolution.

${}^{44}\text{Ti}$  has been detected in supernova remnants [9, 14]. It is produced mainly in the inner ejecta in an  $\alpha$ -rich freeze out of NSE [16]. At high temperatures, photon- and charged particle induced reactions dominate over any neutrino contribution. Therefore, we find no significant effect of neutrinos on the yield of  ${}^{44}\text{Ti}$ . The production of  ${}^{60}\text{Fe}$  in supernovae is discussed in detail in reference [15], where the neutron density reached during the shock is

identified as a key parameter for the yield. Despite the increase in the density of free nucleons due to neutrino spallation reactions, we find no significant modification of the  $^{60}\text{Fe}$  yield.

Reference [37] has discussed the  $\nu$  process in supernovae as a production site for the radioactive isotopes  $^{92}\text{Nb}$  and  $^{98}\text{Tc}$ . Our calculations show, that charged-current neutrino interactions increase the yield of  $^{92}\text{Nb}$  on average by a factor of 35. The yield of  $^{98}\text{Tc}$  is increased by only 17%-21% for the  $15 M_{\odot}$  and the  $20 M_{\odot}$  progenitors. For the more massive stars however, the enhancement goes up to a factor of 100, such that the total yield for all of the progenitors is between  $1 \times 10^{-11} M_{\odot}$  and  $6 \times 10^{-11} M_{\odot}$ . The yields for these nuclei might even be more enhanced by contributions from the neutrino-driven wind [38].

We have performed an updated study of  $\nu$  process nucleosynthesis. Compared to previous studies, we use a full set of neutrino-induced charged- and neutral current reactions including spallation products for nuclei with charge numbers  $Z < 76$ . Additionally, we use neutrino spectra for all neutrino flavors that are consistent with recent supernova simulations [19–21] that predict noticeably lower average energies particularly for  $\mu$  and  $\tau$  (anti)neutrinos. Despite the lower average energy, we confirm the production of  $^7\text{Li}$ ,  $^{11}\text{B}$ ,  $^{138}\text{La}$ , and  $^{180}\text{Ta}$  by neutrino nucleosynthesis, albeit at slightly smaller abundances due to the changed neutrino spectra. We find that neutrino-induced reactions, either directly or indirectly, contribute to the production of long-lived radioactive nuclei. The yields of  $^{22}\text{Na}$  and  $^{26}\text{Al}$ , both prime candidates for gamma-ray astronomy, are noticeably enhanced. As a consequence of the reduced neutrino energies, we find that the role of charged current reactions is enhanced with respect to previous studies [11, 18]. The relevant neutrino-nucleus cross-sections rely almost entirely on theoretical calculations and are therefore accompanied by large uncertainties. Experimental data on the relevant transitions could help to reduce the uncertainties in order to make inferences from observations more reliable. Furthermore, important uncertainties remain related to the progenitor structure [16], helium burning rates [39], and the long term evolution of the neutrino spectra and neutrino oscillations [40].

We thank Yong-Zhong Qian and Meng-Ru Wu for useful discussions. This work was partly supported by the Deutsche Forschungsgemeinschaft through contract SFB 634, the Helmholtz International Center for FAIR within the framework of the LOEWE program launched by the state of Hesse, and the Helmholtz Association through the Nuclear Astrophysics Virtual Institute (VH-VI-417). AH was supported by an Australian Research Council (ARC) Future Fellowship (FT120100363).

- 
- [1] E. M. Burbidge, G. R. Burbidge, W. A. Fowler, and F. Hoyle, *Rev. Mod. Phys.* **29**, 547 (1957).
  - [2] A. G. W. Cameron, *Stellar Evolution, Nuclear Astrophysics, and Nucleogenesis*, Report CRL-41 (Chalk River, 1957).
  - [3] M. Wiescher, F. Käppeler, and K. Langanke, *Annu. Rev. Astron. Astrophys.* **50**, 165 (2012).
  - [4] F.-K. Thielemann *et al.*, *Prog. Part. Nucl. Phys.* **66**, 346 (2011).
  - [5] M. Arnould and K. Takahashi, *Rep. Prog. Phys.* **62**, 395 (1999).
  - [6] K. Langanke and H. Schatz, *Phys. Scr.* **T152**, 014011 (2013).
  - [7] C. Winkler, R. Diehl, P. Ubertini, and J. Wilms, *Space Sci. Rev.* **161**, 149 (2011).
  - [8] R. Diehl *et al.*, *Nature* **439**, 45 (2006).
  - [9] B. W. Grefenstette *et al.*, *Nature* **506**, 339 (2014).
  - [10] R. Diehl, *Astron. Rev.* **8**, 19 (2013).
  - [11] S. E. Woosley, D. H. Hartmann, R. D. Hoffman, and W. C. Haxton, *Astrophys. J.* **356**, 272 (1990).
  - [12] F. X. Timmes, S. E. Woosley, D. H. Hartmann, R. D. Hoffman, T. A. Weaver, and F. Matteucci, *Astrophys. J.* **449**, 204 (1995).
  - [13] R. Diehl and F. X. Timmes, *Publ. Astron. Soc. Pacific* **110**, 637 (1998).
  - [14] A. F. Iyudin, R. Diehl, H. Bloemen, W. Hermsen, G. G. Lichti, D. Morris, J. Ryan, V. Schönfelder, H. Steinle, M. Varendorff, C. de Vries, and C. Winkler, *Astron. & Astrophys.* **284**, L1 (1994).
  - [15] M. Limongi and A. Chieffi, *Astrophys. J.* **647**, 483 (2006).
  - [16] S. E. Woosley, A. Heger, and T. A. Weaver, *Rev. Mod. Phys.* **74**, 1015 (2002).
  - [17] T. Rauscher, A. Heger, R. D. Hoffman, and S. E. Woosley, *Astrophys. J.* **576**, 323 (2002).
  - [18] A. Heger, E. Kolbe, W. Haxton, K. Langanke, G. Martínez-Pinedo, and S. E. Woosley, *Phys. Lett. B* **606**, 258 (2005).
  - [19] L. Hüdepohl, B. Müller, H. Janka, A. Marek, and G. G. Raffelt, *Phys. Rev. Lett.* **104**, 251101 (2010).
  - [20] G. Martínez-Pinedo, T. Fischer, A. Lohs, and L. Huther, *Phys. Rev. Lett.* **109**, 251104 (2012).
  - [21] G. Martínez-Pinedo, T. Fischer, and L. Huther, *J. Phys. G: Nucl. Part. Phys.* **41**, 044008 (2014).
  - [22] E. Kolbe, K. Langanke, S. Krewald, and F.-K. Thielemann, *Nucl. Phys. A* **540**, 599 (1992).
  - [23] E. Kolbe, K. Langanke, G. Martínez-Pinedo, and P. Vogel, *J. Phys. G: Nucl. Part. Phys.* **29**, 2569 (2003).
  - [24] H. P. Loens, Ph.D. thesis, TU Darmstadt (2010).
  - [25] A. Kelic, M. Valentina Ricciardi, and K.-H. Schmidt, ArXiv e-prints (2009), [arXiv:0906.4193 \[nucl-th\]](https://arxiv.org/abs/0906.4193).
  - [26] D. Gazit and N. Barnea, *Phys. Rev. Lett.* **98**, 192501 (2007).
  - [27] A. Byelikov *et al.*, *Phys. Rev. Lett.* **98**, 082501 (2007).
  - [28] [http://2sn.org/nucleosynthesis/presn\\_comp.shtml](http://2sn.org/nucleosynthesis/presn_comp.shtml).
  - [29] S. E. Woosley and T. A. Weaver, *Astrophys. J. Suppl.* **101**, 181 (1995).
  - [30] S. Horiuchi, K. Nakamura, T. Takiwaki, K. Kotake, and M. Tanaka, *Mon. Not. Roy. Ast. Soc.* **445**, L99 (2014).
  - [31] T. Sukhbold and S. E. Woosley, *Astrophys. J.* **783**, 10 (2014).
  - [32] T. Ertl, H.-T. Janka, S. E. Woosley, T. Sukhbold, and

- M. Ugliano, ArXiv e-prints (2015), [arXiv:1503.07522](https://arxiv.org/abs/1503.07522) [[astro-ph.SR](https://arxiv.org/archive/astro-ph)].
- [33] T. Fischer, S. C. Whitehouse, A. Mezzacappa, F.-K. Thielemann, and M. Liebendörfer, *Astron. & Astrophys.* **499**, 1 (2009).
- [34] K. Lodders, *Astrophys. J.* **591**, 1220 (2003).
- [35] A. Heger and S. E. Woosley, *Astrophys. J.* **724**, 341 (2010).
- [36] [http://www.iasf-roma.inaf.it/orfeo/public\\_html](http://www.iasf-roma.inaf.it/orfeo/public_html).
- [37] M.-K. Cheoun, E. Ha, T. Hayakawa, S. Chiba, K. Nakamura, T. Kajino, and G. J. Mathews, *Phys. Rev. C* **85**, 065807 (2012).
- [38] G. M. Fuller and B. S. Meyer, *Astrophys. J.* **453**, 792 (1995); R. D. Hoffman, S. E. Woosley, G. M. Fuller, and B. S. Meyer, *Astrophys. J.* **460**, 478 (1996).
- [39] S. M. Austin, C. West, and A. Heger, *Phys. Rev. Lett.* **112**, 111101 (2014).
- [40] M.-R. Wu, Y.-Z. Qian, G. Martínez-Pinedo, T. Fischer, and L. Huther, *Phys. Rev. D* **91**, 065016 (2015).